Microfluidics and Nanofluidics (2018) 22:7
https://doi.org/10.1007/s10404-017-2027-z

RESEARCH PAPER

Surface charge-dependent transport of water in graphene nano-channels

Alper Tunga Celebi[1] · **Murat Barisik**[2] · **Ali Beskok**[1]

Received: 16 October 2017 / Accepted: 5 December 2017 / Published online: 11 December 2017

Abstract
Deionized water flow through positively charged graphene nano-channels is investigated using molecular dynamics simulations as a function of the surface charge density. Due to the net electric charge, Ewald summation algorithm cannot be used for modeling long-range Coulomb interactions. Instead, the cutoff distance used for Coulomb forces is systematically increased until the density distribution and orientation of water atoms converged to a unified profile. Liquid density near the walls increases with increased surface charge density, and the water molecules reorient their dipoles with oxygen atoms facing the positively charged surfaces. This effect weakens away from the charged surfaces. Force-driven water flows in graphene nano-channels exhibit slip lengths over 60 nm, which result in plug-like velocity profiles in sufficiently small nano-channels. With increased surface charge density, the slip length decreases and the apparent viscosity of water increases, leading to parabolic velocity profiles and decreased flow rates. Results of this study are relevant for water desalination applications, where optimization of the surface charge for ion removal with maximum flow rate is desired.

Keywords Surface charge density · Slip length · Viscosity · MD simulation of electrically charged systems

1 Introduction

Nano-fluidic systems can provide significant advantages in addressing our industrial, agricultural and drinking water needs. For example, "tunable nano-membranes" can be developed to provide cost-effective water deionization and desalination techniques where the membrane surface charge can be modified to remove specific ionic species from pressure-driven water flows, either by chemical alteration of the surface functional groups or using gated electrodes (Cohen-Tanugi and Grossman 2012; Mahmoud et al. 2015). However, the surface charges may significantly alter water flow inside the nano-confinements. Proper assessment of the "tunable nano-membrane" technology requires enhanced understanding of water transport as a function of the surface charge.

✉ Ali Beskok
abeskok@smu.edu

[1] Lyle School of Engineering, Southern Methodist University, Dallas, TX, USA

[2] Department of Mechanical Engineering, Izmir Institute of Technology, Izmir, Turkey

Molecular surface force-fields and confinement affect liquid transport in nanoscale systems (Karniadakis et al. 2005). The major mechanism induced by surface forces is density layering of liquids near the walls that extends several molecular diameters in the near-surface region (Koplik and Banavar 1995). Liquid molecules undergo solid-like ordering near the walls which ultimately determines the liquid/solid momentum exchange at the interface (Li et al. 2010). Depending on the liquid/solid interaction strength, liquid may exhibit velocity slip, no-slip or adsorption (Koklu et al. 2017). Also the channel-averaged fluid density and apparent viscosity deviate from their thermodynamic bulk values (Ghorbanian and Beskok 2016; Karniadakis et al. 2005). The fluid density and flow exhibit continuum behavior only sufficiently away from the surfaces (Lyklema 2005). As a result, predictions of the continuum transport models become inaccurate with reduced channel size, and ultimately discrete transport of liquid molecules under the influence of wall force field dominates the transport (Joseph and Aluru 2008).

The influences of velocity slip and apparent viscosity on nanoscale water transport have been studied extensively (Kumar Kannam et al. 2012; Nagayama and Cheng 2004; Vo et al. 2015). Water flow through graphene nano-channels and tubes exhibit ultra-fast transport due to the

large slip lengths and increased structural order of water in nano-confinements (Falk et al. 2010; Nicholls et al. 2012; Radha et al. 2016). These behaviors promoted use of graphene-based materials for nano-membrane applications (Chen et al. 2017a; Wei et al. 2014b; Xu et al. 2017). However, a breakdown of flow rate enhancement was observed in the cases of chemical functionalization or oxidation of the surfaces (Chen et al. 2017b; Montessori et al. 2017; Wei et al. 2014a). Many desalination applications use Coulomb forces to repel ions by adjusting the surface charges inside or at the entrance of the nano-membranes (Chan and Ren 2016). Unfortunately, the surface charges required for selective ion passage decrease the flow rate of purified water and increase the pressure drop required to maintain the desired flow rate (Xiao et al. 2016).

The effects of surface charge on liquid/surface interactions were investigated in terms of surface wetting. Variation of both static wettability and wetting kinetics was observed as a function of surface charge density (Puah et al. 2010). Molecular dynamics (MD) studies of nano-droplets on charged surfaces showed enhancement of surface wettability with increased charge density, where the wetting angle decreased and the surface became more hydrophilic, corresponding to stronger liquid–solid interactions (Giovambattista et al. 2007). Polarizable water molecules reorient themselves on a charged surface. Increasing the surface charge magnitude aligns the dipole moments of water molecules and restricts their degree of freedom (Daub et al. 2007; Ho and Striolo 2013). This effect can be crucial in nanoscale confinements and significantly alter the momentum exchange of liquid molecules.

Recently, we investigated deionized water flow through graphene nano-channels subjected to opposing surface charges and have shown that the resulting electric field-induced asymmetric density distribution and velocity profiles in the channels (Celebi et al. 2017). With increased electric fields, slip length decreased and the apparent viscosity increased, while electro-freezing of water was observed above a certain threshold value. Results indicated the possibility of using oppositely charged graphene nano-channels for flow control applications (Celebi et al. 2017). Current study distinguishes itself due to use of graphene nano-channels subjected to identical positive electric charges. For such a case, charged graphene surfaces act as gated electrodes, which might significantly alter the flow. Although lack of dissolved salts and H^+ and OH^- ions avoids electric double-layer formation, the number of free ions in nano-channels is often very small, and their presence does not greatly affect force-driven flows. Therefore, the current study closely mimics water desalination or deionization processes using graphene nano-channel surfaces as gated electrodes, while avoiding additional complexities of modeling ionized fluids.

To the best of our knowledge, the effects of surface electric charge on the structure and dynamics of water have not been previously reported in the literature. Thus, we carried out non-equilibrium molecular dynamics (NEMD) simulations for force-driven water flow through identically charged planar graphene surfaces. The primary objective of the present study is to investigate the effect of surface charge density on the structural and transport properties of water in graphene nano-confinements at a length scale, where the continuum behavior is still valid. We principally focus on the density distributions, molecular orientations, velocity profiles, viscosities, slip lengths and flow rates after ensuring a fixed thermodynamic state. A unique computational aspect of this work is the use of large cutoff distances to model Coulomb interactions between charged molecules, since Ewald summation algorithm is inapplicable for simulation systems with a net electric charge.

2 Theoretical background

We consider force-driven water flow in charged graphene nano-channels as illustrated in Fig. 1 and investigate variations in the slip length and viscosity of water using continuum transport theory. For steady, incompressible, fully developed and force-driven Newtonian fluid flows, the Navier–Stokes equation is reduced to

$$\frac{\mathrm{d}^2 u}{\mathrm{d}z^2} = -\frac{f}{\mu} \tag{1}$$

where $u(z)$, f and μ are the velocity field, driving force and the fluid viscosity, respectively. We consider a Navier-type slip boundary condition at the liquid–solid interface as follows

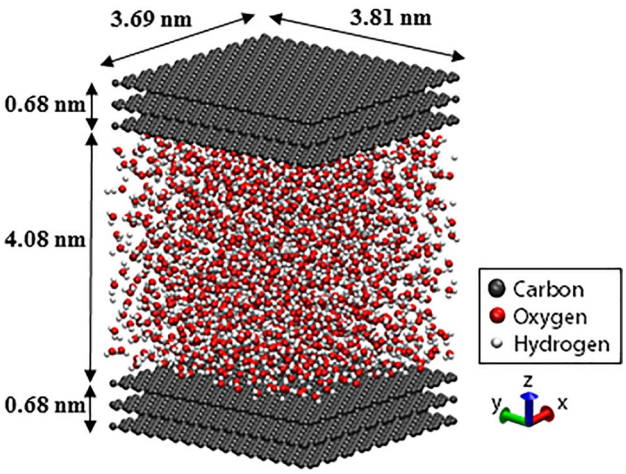

Fig. 1 Schematic representation of simulation domain

$$u_s - u_w = \beta \frac{\mathrm{d}u}{\mathrm{d}z} \tag{2}$$

where β is the slip length, u_s is the slip velocity and u_w is the wall velocity. Using a constant slip length on both surfaces ($z = 0$ and $z = h$), velocity distribution in the channel is given by

$$u(z) = \frac{fh^2}{2\mu}\left(-\left(\frac{z}{h}\right)^2 + \left(\frac{z}{h}\right) + \left(\frac{\beta}{h}\right)\right) \tag{3}$$

We apply a polynomial fit approach using the velocity profiles obtained from MD simulations in order to find the slip length and water viscosity (Backer et al. 2005; Ghorbanian et al. 2016). Initially, a second-order polynomial equation in the form of $u(z) = Az^2 + Bz + C$ is fitted to the averaged MD velocity profile. Then, the coefficients (A, B and C) of this fit are compared with the analytical solution given in Eq. 3. Fluid viscosity is found by

$$\mu = -\frac{f}{2A} \text{ and } \mu = -\frac{fh}{2B} \tag{4}$$

These two viscosity values are equal to each other when the velocity distribution is symmetric. Furthermore, the slip length is calculated using the coefficient C by

$$\beta = \frac{2C\mu}{fh} \tag{5}$$

This curve-fitting method yields good estimate of viscosity and slip length for parabolic velocity profiles. However, the approach becomes inadequate for plug-like velocity profiles, where polynomial fitting induces large statistical errors (Kumar Kannam et al. 2012). For such cases, one can relate the wall shear (τ_w) to the total body force exerted on water molecules using conservation of linear momentum in the flow direction as $\tau_w = \frac{fh}{2}$. Combining this equation with Navier-type slip equation given in Eq. 2 and the constitutive law for Newtonian fluids ($\tau_w = \mu\frac{\mathrm{d}u}{\mathrm{d}y}$), we obtain the slip length as follows

$$\beta = \frac{2\mu u_s}{fh} \approx \frac{2\mu\bar{u}}{fh} \tag{6}$$

where u_s is the slip velocity and $\bar{u}$ is the channel average velocity. For plug-like velocity profile, the slip velocity is practically equal to the average velocity (Falk et al. 2010).

3 Molecular dynamics simulation

The three-dimensional model consists of liquid water molecules confined between two solid graphitic walls as shown in Fig. 1. Each wall is made of three graphene layers which were placed 3.4 Å apart from each other. Graphene sheets were oriented on the XY plane with a Bernal (ABA) stacking arrangement (Yacoby 2011). Dimensions of the simulation domain were set as 3.69 × 3.81 × 5.44 nm in the lateral (x) and longitudinal (y) and vertical (z) directions, respectively. In this study, we specifically picked a channel height of $h = 4.08$ nm, which is large enough to exhibit a substantial bulk region around the channel center and density layering near the walls due to wall force field effects. In much narrower channels, description of the thermodynamic state breaks down and water molecules experience discrete molecular transport. Hence, derivation of continuum properties such as density, velocity and viscosity becomes irrelevant (Travis et al. 1997). Our previous studies have shown that the continuum flow theory can be used to predict the properties of bulk water at a known thermodynamic state for channel heights as small as 2–3 nm (Ghorbanian and Beskok 2016; Ghorbanian et al. 2016). Qiao and Aluru also presented that continuum predictions can still hold up to the channel heights of 2.2 nm (Qiao and Aluru 2003).

Intermolecular interactions between all atomic pairs were modeled using Lennard-Jones (LJ) and Coulomb potentials given by,

$$\emptyset(r_{ij}) = 4\epsilon\left[\left(\frac{\sigma_{ij}}{r_{ij}}\right)^{12} - \left(\frac{\sigma_{ij}}{r_{ij}}\right)^{6}\right] + \frac{1}{4\pi\epsilon_0}\sum_{i}^{a}\sum_{j}^{b}\frac{q_i q_j}{r_{ij}} \tag{7}$$

where ϵ is the well-depth, σ is the van der Waals distance, ϵ_0 is the vacuum permittivity, q_i are the partial charges, r_{ij} are the distance between charged species. Potential parameters between all atomic species are summarized in Table 1.

Water molecules were modeled using a rigid four-site TIP4P/2005 model (Abascal and Vega 2005). Bond lengths and angle of water molecules were kept rigid using SHAKE algorithm (Miyamoto and Kollman 1992). We only considered the LJ interactions of oxygen atom in a water molecule, assuming hydrogen's contribution is negligible due to its much smaller mass and size. Interactions between carbon and oxygen atoms were calculated based on the parameters obtained by experimental study of Werder et al. (Werder et al. 2003). We excluded the interaction between carbon atoms to attain a rigid (cold) wall behavior, which provides substantial enhancement in the computational efficiency (Thomas et al. 2010). Only the carbon atoms at the innermost layers of graphene channels were modeled as charged

Table 1 Potential parameters for atomic pairs

Atom pair	σ (nm)	ϵ (kj/mol)	q (e)
H–H	0	0	0.5564
O–O	0.31589	0.7749	− 1.1128 (dummy)
C–O	0.3190	0.3921	Varies

particles, while the remaining carbon atoms were neutral. We used a cutoff distance of 1 nm for all LJ calculations ($r_{C-LJ} = 1$ nm).

One of the main challenges we faced during this study was the calculation of long-range Coulomb intermolecular forces. Our system consists of water molecules carrying equal amounts of positive and negative charges, and carbon molecules having positive charges only. This results in a system with a positive net charge. Ewald summation algorithm is frequently used to calculate the long-range part of Coulomb forces beyond the cutoff distance (r_{C-Coul}; Ewald 1921). However, this algorithm was developed with the assumption that the net charge of the system is zero. For systems with a net electric charge, the Ewald summation algorithms, such as Particle-Particle-Particle-Mesh (PPPM) (Hockney and Eastwood 1988), add additional phantom-charges to make the system neutral in order to bring the simulation to a state at which algorithm is applicable (Plimpton et al. 1997). This creates an artificial force on simulated molecules and develops unphysical behaviors (Ballenegger et al. 2009; Bogusz et al. 1998; Hub et al. 2014). In order to simulate a system with a net electric charge, we systematically increased the cutoff distance employed at different surface charge density cases and examined the resulting water density profiles, as shown in Fig. 2a. Systematically increasing the cutoff distance, density distribution of water converged to a unified profile when the cutoff distance became equal to or higher than the simulated channel height of 4.08 nm. Results obtained using PPPM with 1-nm cutoff distance are also shown in the figure and exhibit wrong density profile due to electro-neutrality induced by the Ewald summation algorithm. As the cutoff length reached the domain size, force interactions of any molecule with every other molecule in the domain and its own image on the periodic surfaces could be calculated properly. In order to validate the results obtained using $r_{C-Coul} = 4$ nm, we performed further simulations, where the net system charge was neutralized by adding ions with opposite charges to the imposed surface charge. For such cases, the well-known PPPM algorithm with $r_{C-Coul} = 1$ nm was appropriately employed for calculating the Coulomb forces. Since the number of ions added for neutralization of low-surface-charge cases was small and had negligible effects, water densities for low-surface-charge cases showed good agreement between $r_{C-Coul} = 4$ nm without PPPM and $r_{C-Coul} = 1$ nm using PPPM (Fig. 2b). However, high surface charges required addition of large number of ions, which started affecting the water density profiles, and comparisons with the density profiles of water with no ions became unreasonable. Overall, we validated the results of $r_{C-Coul} = 4$ nm using a cutoff distance dependence study and an agreement is obtained with the results of PPPM at low-surface-charge systems neutralized by addition of ions. Therefore, Coulomb interactions between all charged particles were calculated properly using 4-nm cutoff distance.

This study uses Large-Scale Atomic/Molecular Massively Parallel Simulator (LAMMPS) (Plimpton 1995). Periodic boundary conditions were applied in x and y directions. Initially, each system achieved thermal equilibrium in a Canonical (NVT) ensemble before being subjected to any driving forces. For this purpose, initial velocities of each water molecule were randomly assigned by imposing a Gaussian distribution based on the specified temperature. Then, the MD system was run for 1 ns using 1-fs time steps to reach an equilibrium state in absence of external forces. The thermodynamic state was fixed by maintaining the temperature of water at 300 K using Nose–Hoover thermostat and keeping the bulk density of water at 997 kg/m^3. Temperature was computed from the total kinetic energy, and the equilibrium state was verified.

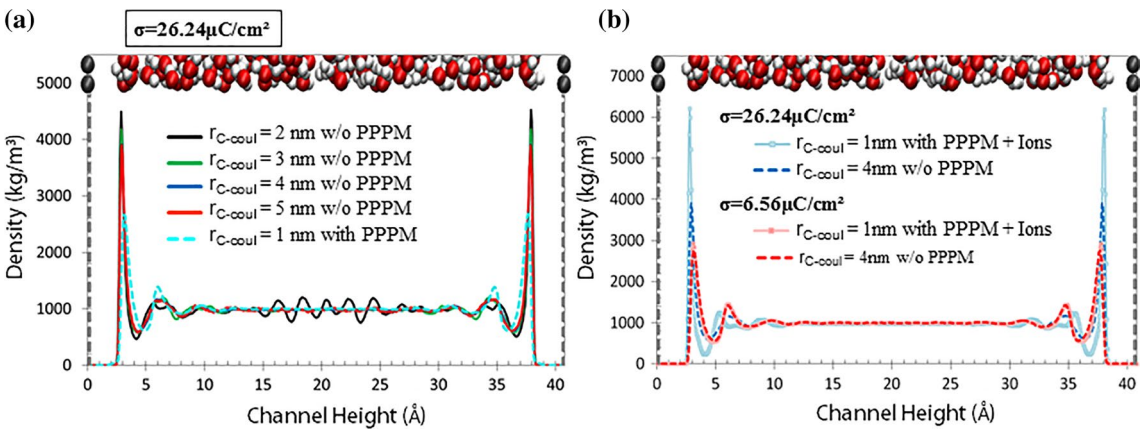

Fig. 2 **a** Density distribution in a charged channel calculated using PPPM with $r_{C-Coul} = 1$ nm, compared to distributions of $r_{C-Coul} = 2$, 3, 4 and 5 nm cases without PPPM. **b** Density distributions at different surface charges obtained by $r_{C-Coul} = 4$ nm and using PPPM with $r_{C-Coul} = 1$ nm and ion addition

Next, force-driven water flow simulations were performed starting from the equilibrium conditions. Flow simulations employ Nose–Hoover thermostat on the degrees of freedoms perpendicular to the flow direction. The flow was driven by an external force in y-direction imposed on each atom of the water molecule based on their mass. In order to avoid the nonlinear effects, the magnitude of the body force for each surface charge density case was selected to limit the maximum water velocities under 60 m/s (Binder et al. 2004; Sofos et al. 2009). We determined this linear response regime by systematically investigating the average channel velocity as a function of the driving force (not shown for brevity). Time scale for momentum diffusion was estimated using $t_d \approx h^2/v$, where h and v are the channel height and kinematic viscosity, respectively (Ghorbanian et al. 2016). Steady flow was ensured by initially running the system for 1 ns, which corresponds to $6t_d$. Subsequently, an additional 6 ns was performed for data collection and statistical averaging, which creates 800 independent time-averaged data sets. In order to obtain better resolution at the graphene–water interface, we divided the simulation box into 1200 bins in the direction of the channel height.

4 Results

We first investigate the density distributions of water between positively charged graphene nano-channels. To generate uniform surface charge density (σ), we assigned single point charges to each carbon atom in the innermost layer of each graphitic wall. In the current study, we used surface charge densities of 0, 6.56, 13.12, 19.68 and 26.24 μC/cm^2 based on the values reported in similar MD studies (Kalluri et al. 2011; Xia and Berkowitz 1995). Such surface charge densities are relatively high, but not totally impractical (Israelachvili 2015; Qiao and Aluru 2004). Figure 3 shows water density profiles obtained under five different surface charges. A constant density region is observed in the middle of channel with three apparent density layering near each wall due to the wall–liquid attraction and volume exclusion effects (Koplik and Banavar 1995). The thermodynamic state for all five cases is identical since the water reaches a constant density of 997 kg/m^3 in the bulk region, and the system is kept at $T = 300$ K. Results show increased water density in the near-wall region with increased surface charge, indicating enhanced surface wetting. Density profiles show an empty region between the first water density peak and the wall center. This region is about $L_O \approx 0.3$ nm thick, which is not negligible compared to the channel height of $h = 4.08$ nm. Since water molecules concentrate at the first density peak, L_O also defines the slip plane for flow studies. In (Ghorbanian et al. 2016), we define an effective channel

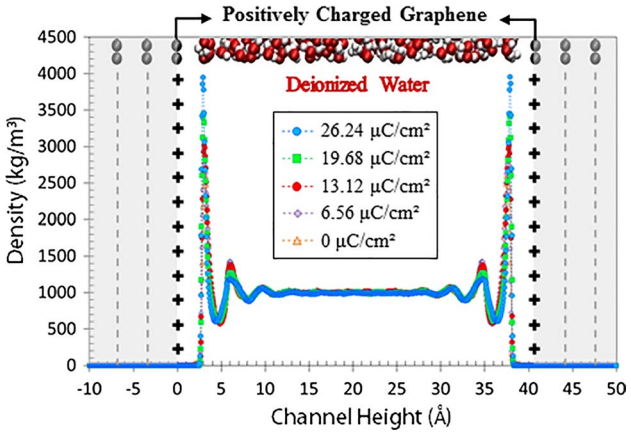

Fig. 3 Water density profiles obtained for different surface charge densities

height as $h_e = h - 2L_O$ and base all continuum calculations on the effective channel height.

To elucidate the interfacial density behavior, we examine the density profiles within 1-nm distance from the wall in Fig. 4. We only present the results near one wall because the density distributions near both walls are the same. Magnitude of the first density peak increases with increased surface charge. This is a result of higher interfacial energy and stronger wall–fluid interactions that increase the number of molecules at the first hydration layer. On the other hand, the second density peaks are reduced as the surface charge increases, while the third density peaks do not show any variation as a function of the surface charge. Furthermore, surface charge also alters the location of the density peaks. At $\sigma = 26.24$ μC/cm^2, the first density peak is formed approximately at $L_O = 2.94$ Å, while the peak was at $L_O = 3.16$ Å for the uncharged case. Current findings agree with the results reported earlier (Ho and Striolo 2013). Figure 4b shows oxygen and hydrogen densities normalized by their average values. Due to the Coulomb forces from the positive surface charges, oxygen molecules are located closer to the surface within the first two density peaks.

Oxygen and hydrogen density distributions suggest that applied surface charges have substantial effect on the orientation of water molecules. We calculated the probability distribution of water molecules using a prescribed angle approximation in order to quantify these molecular orientations. We defined angle θ between dipole vector of a water molecule and the surface normal vector as shown in Fig. 5 (Cipcigan et al. 2015). The angle becomes 0° when the molecular dipole vector points away from the wall, while it becomes 180° when the molecular dipole vector points toward the surface. Therefore, the probability distribution varies between + 1 and − 1 depending on the angle. In Fig. 5, we present the probability distribution and angle

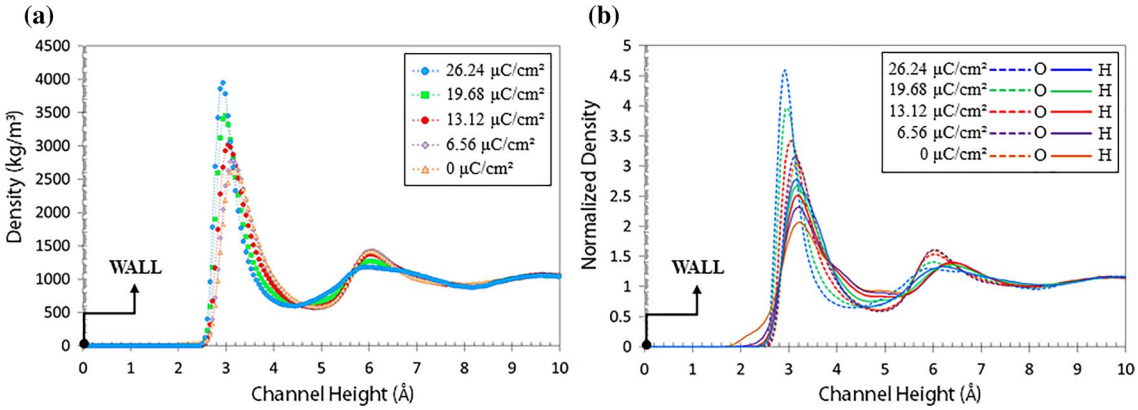

Fig. 4 **a** Water density distribution within 1 nm of the positively charged surface; **b** distribution of normalized oxygen and hydrogen densities within 1 nm of the surface

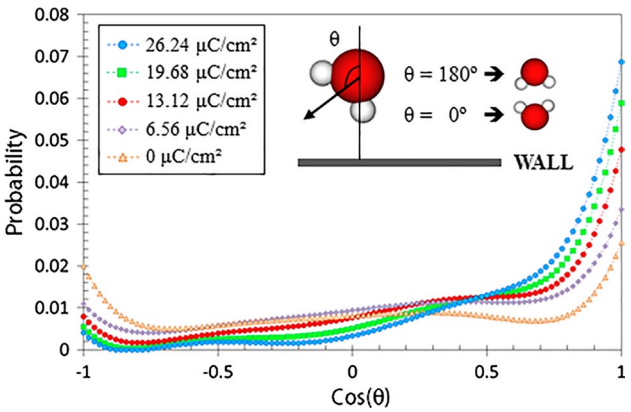

Fig. 5 Probability distribution of water molecules at the interface for different wall charges

cosines of interfacial water molecules at different surface charge densities. Similar to the earlier studies in the literature (Ho and Striolo 2014; Lee et al. 1984), we only considered water molecules within the first hydration layer, which is 0.5-nm distance from the wall. The probability of water molecules on a neutral surface shows almost a symmetric distribution where no specific orientations are observed. However, molecular orientations are altered with the surface charge. Positive wall attracts negative oxygen atoms and repels positive hydrogen atoms due to Coulomb forces. Therefore, water molecules at the interface rotate their dipole vectors away from the positively charged surfaces with increased electrical charge. As a result, the $\cos(\theta) = 1$ probability increases, corresponding to negatively charged oxygen orienting toward the surface and positively charged hydrogen orienting away from the surface.

Probability distribution of water molecules at different z-locations in the channel is shown in Fig. 6. Water orientations were measured inside every 0.3-nm-thick slabs starting from interfacial water hydration layer of each surface toward the channel center. Results are for the surface charge of 19.68 μC/cm^2. The water dipole moments become more equally distributed by moving away from the surface. Dipole distribution near the channel center is nearly symmetric even for this high-surface-charge case. The orientation of

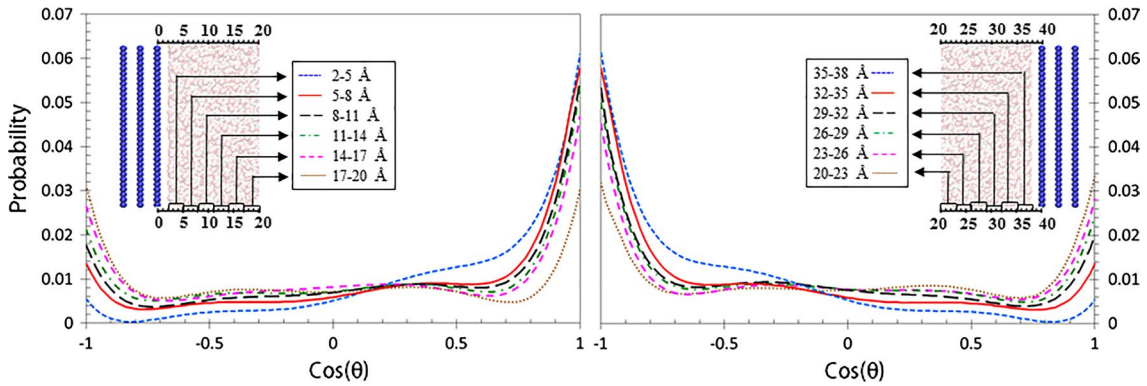

Fig. 6 Probability distribution of water molecules at different proximities to the walls at $\sigma = 19.68$ μC/cm^2

interfacial water molecules near both walls is similar due to the identical electrical charges imposed on each surface.

Figure 7 shows the velocity profiles normalized with their channel-averaged values for different surface charge densities. For zero surface charge, plug-like velocity profile is obtained due to weak interfacial resistance at the water–graphene interface that results in large slip lengths. Slip length normalized with the effective channel height ($\beta^* = \beta/h_e$) determines the shape of the velocity profile in a given channel. Focal length of the parabola increases with increased β^*, exhibiting plug flow behavior for $\beta^* >> 1$ (Ghorbanian et al. 2016). For the zero surface charge case, $\beta^* = 18.4$, and hence, the velocity profile is nearly uniform. Imposing surface electric charges alter the water–graphene interactions and the resulting velocity profiles. Electrical charges on the surface increase the liquid-wall interaction strength, forming parabolic velocity profiles with reduced slip lengths. This effect becomes more prominent with increased surface charge. In addition, the velocity profiles are symmetric with respect to the channel center, implying equal slip lengths on the walls. Using two negatively charged walls also created similar effects (not shown for brevity). The velocity profiles show that surface charges can induce active control of surface wetting and fluid flow in nano-channels.

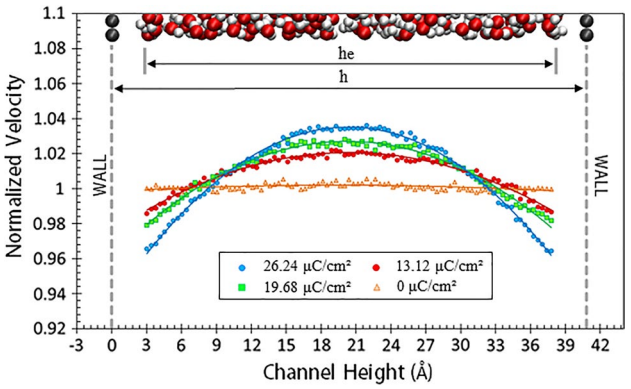

Fig. 7 Velocity profiles for different surface charges

Figure 8 presents the ratio of MD-computed viscosity using Eq. 4 normalized by water viscosity at the given thermodynamic state (μ/μ_{td}), and the MD-computed slip lengths using Eqs. 5 and 6 for different surface charge densities. We targeted for a better understanding of surface charge effects on the transport properties and at the same time assess deviations of the results from continuum predictions. We calculated the viscosity and slip length of each case comparing the velocity profiles obtained from NEMD simulations with well-known continuum Poiseuille flow model. We particularly describe the slip plane at the first water density peak adjacent to the wall. The slip length (β_{SP}) at the slip plane is related to the slip length on the wall (β_W) by $\beta_{SP} = \beta_W + L_O$, where L_O is the distance between the location of the first density peak and the wall. All slip lengths reported in this study are calculated at the slip plane (i.e., $\beta = \beta_{SP}$), where $L_O = 2.94$ Å and $L_O = 3.16$ Å for the $\sigma = 26.24$ μC/cm^2 and $\sigma = 0$ μC/cm^2 cases, respectively.

Increasing the surface charge promotes parabolic velocity distribution due to increasing water–graphene interfacial strength. For $\sigma = 13.12$ μC/cm^2 or larger, velocity profiles exhibit parabolic shapes, where we can easily use the polynomial fit approach in order to predict the viscosities and slip lengths. For $\sigma = 6.56$ μC/cm^2, we applied the plug-like method and polynomial fit approach together to verify our results since the velocity profile presents a small parabolic component. Figure 8 shows viscosity and slip length variations under different surface charge densities. Results exhibit nonlinear increase in water viscosity with increased surface charge density. The absolute viscosity for the largest surface charge density is approximately 1103 μPa s, while it is 863 μPa s for the uncharged surface. Results show drastic reduction in the slip length with increased electrical surface charge. The slip length decreases to 9.7 nm for the largest surface charge density case, exhibiting 6.6-fold reduction. Calculated viscosities and slip lengths are

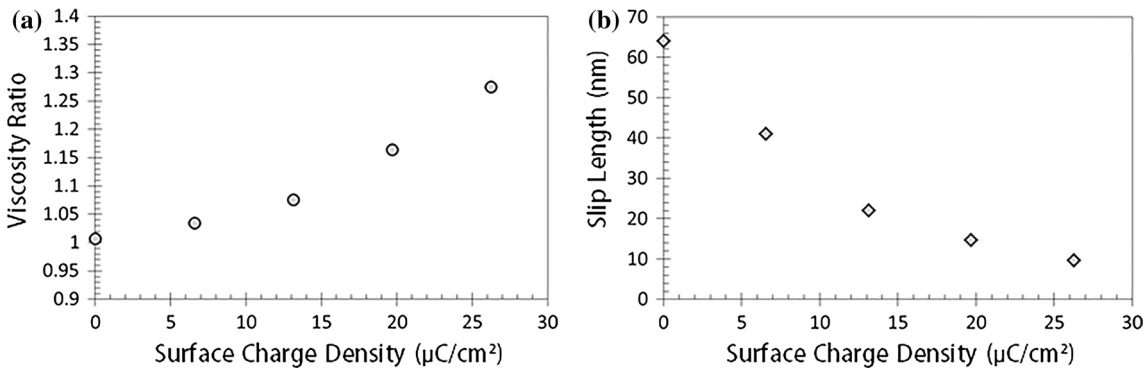

Fig. 8 Variation of the viscosity ratio (μ/μ_{td}) and the slip length as a function of the surface charge density

given in Table 2. Viscosity and slip length results for the uncharged case match well with the data presented in the literature obtained using NEMD and Green–Kubo calculations (Fanourgakis et al. 2012; González and Abascal 2010; Koumoutsakos et al. 2003; Kumar Kannam et al. 2012; Tazi et al. 2012; Xiong et al. 2011). Also calculated viscosity for the uncharged case matches well with the thermodynamic viscosity of water at 300 K (μ_{td} = 855 μPa s). In Table 2, we also present the standard error (SE) values of the slip lengths obtained from 10 independent samples (n) using SE = $S/\sqrt{n}$, where S is the standard deviation. We used 80 consecutive time-averaged data sets to obtain each independent sample. The standard errors in the slip lengths were found in the range of 0.09 to 0.6 for varied surface charge densities.

Decreased slip lengths and increased viscosity due to the surface charge greatly reduce the volumetric flow rate in the channel. In order to obtain speeds suitable for statistical analysis, we increased the driving force applied on each atom for the increased surface charge cases. The driving forces (f) and the resulting volumetric flow rates ($\dot{Q}_{\mathrm{MD}}$) are also presented in Table 2. Since the volumetric flow rate is linearly dependent on the driving force, different surface charge cases can be compared with each other using normalized flow rate. First, we divide volumetric flow rate by the driving force to obtain $\dot{q}_{\mathrm{MD}} = \dot{Q}_{\mathrm{MD}}/f$. Normalizing $\dot{q}_{\mathrm{MD}}$ data with the value of the electrically neutral case, we obtained $\dot{q}^*_{\mathrm{MD}}$. Figure 9 shows variation of $\dot{q}^*_{\mathrm{MD}}$ as a function of the surface charge density. As can be seen in the figure, the normalized volumetric flow rate is reduced to 13.2% of the neutral graphene channel for the 26.24 μC/cm^2 case. Theoretical prediction of the volumetric flow rate based on continuum equations is given by

$$\dot{Q}_T = \frac{f h_e^3 w}{12\mu}(1 + 6\beta^*) \tag{8}$$

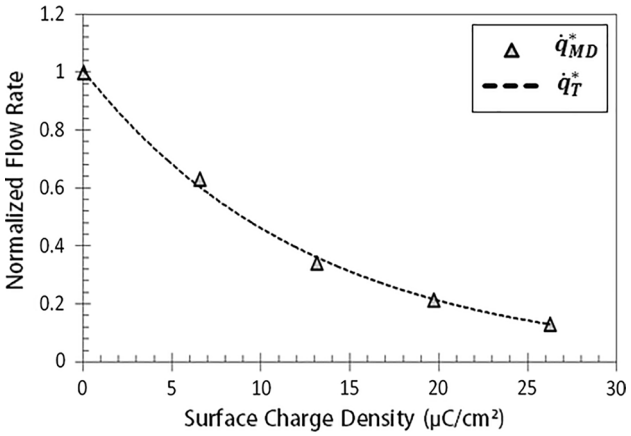

Fig. 9 Normalized MD volumetric flow rate and normalized theoretical flow rate Eq. 9 as a function of the surface charge density

Volumetric flow rates predicted by Eq. 8 are also given in Table 2 using the MD-calculated slip lengths and viscosities. Normalizing the flow rate for all charged surface cases ($\dot{Q}_{T\sigma}$) with the electrically neutral case $\dot{Q}_{Tn}$ under constant driving force f gives

$$\dot{q}^*_T = \frac{\dot{Q}_{T\sigma}}{\dot{Q}_{Tn}} = \left(\frac{\mu_n}{\mu_\sigma}\right)\left(\frac{1 + 6\beta^*_\sigma}{1 + 6\beta^*_n}\right) \tag{9}$$

where the subscripts σ and n show the electrically charged and neutral cases, respectively. Using the slip length and viscosity data reported in Table 2, we present in Fig. 9 the predictions of Eq. 9 using solid line. Good match between the normalized MD data and Eq. 9 is observed. It is important to indicate that this match does not imply the validity of continuum equations for 4-nm-height graphene channel. Comparison of the continuum predicted and MD-calculated volumetric flow rates in Table 2 show up to 5.5% difference due to the scale effects. The reasons of these deviations and a phenomenological continuum model appropriate for these length scales were previously described in (Ghorbanian et al. 2016).

Table 2 Transport parameters at different surface charges

Surface charge (μC/cm^2)	Viscosity (μPa s)	Slip length (nm)	Driving force (N)	β^*	$\dot{Q}_{\mathrm{MD}}$ (m^3/s)	$\dot{Q}_T$ (m^3/s)	$\dot{q}^*_{\mathrm{MD}}$	$\dot{q}^*_T$
26.24	1103.1	9.68 ± 0.09	2.07×10^{-10}	2.79	8.86×10^{-16}	8.41×10^{-16}	0.132	0.126
19.68	1001.7	14.8 ± 0.2	1.25×10^{-10}	4.26	8.77×10^{-16}	8.29×10^{-16}	0.217	0.211
13.12	926.7	22.1 ± 0.4	6.70×10^{-11}	6.35	7.44×10^{-16}	7.06×10^{-16}	0.342	0.338
6.56	886.3	41.5 ± 0.6	3.05×10^{-11}	11.9	6.23×10^{-16}	6.18×10^{-16}	0.631	0.627
0	863.4	64.1 ± 0.6	2.74×10^{-11}	18.4	8.88×10^{-16}	8.66×10^{-16}	1	1

MD measured volumetric flowrate $\dot{Q}_{\mathrm{MD}}$ compared with theoretical predictions from Eq. 8 using the viscosity and slip lengths calculated by MD $\dot{Q}_T$; normalized MD flowrate ($\dot{q}^*_{MD}$) and theoretical flowrate $\left(\dot{q}^*_T\right)$ from Eq. 9

5 Conclusions

Force-driven water flows in graphene nano-channels with positive surface charges are investigated using MD simulations. Frequently used Ewald summation algorithms exhibit non-physical behavior due to the finite electric charge in the simulations. This difficulty is surpassed by using a Coulomb force cutoff length equal to the simulated system size. Surface charge alters the surface wetting and transport characteristics of water in the channel. Basically, electrostatic forces contribute to water layering near the surface and further develop a preferred alignment of dipolar water molecules in the near-surface region. An increase in charge density increases the water density peaks and brings them closer to the interface, while more water molecules orient their dipoles opposite to the surface in case of a positive surface charge. As a result, force-driven flows exhibit increased water viscosity and decreased slip lengths. For example, the slip length of water on graphene surfaces at $\sigma = 26.24$ μC/cm^2 is 6.6 times smaller than that of the electrically neutral surfaces, and the water viscosity increases nearly 29% from its thermodynamic value. Volumetric flow rates present the overall influence of surface charge on the water transport. With the increase in surface charge, flow rate is reduced to almost 13.2% of the neutral graphene channel for the $\sigma = 26.24$ μC/cm^2 case. We theoretically predict flow rates using MD-calculated viscosity and slip values and a continuum model based on the effective channel height with 0.8–5.5% error. Overall, the results show reduced transport inside charged graphitic surfaces, which is an undesired outcome for charged surface nano-membrane applications. For example, the applied electric charge used to separate ionic species can substantially decrease the flow rate. These findings are important for optimization of selective ion transport nano-channels and membranes.

References

Abascal JL, Vega C (2005) A general purpose model for the condensed phases of water: TIP4P/2005. J Chem Phys 123:234505

Backer J, Lowe C, Hoefsloot H, Iedema P (2005) Poiseuille flow to measure the viscosity of particle model fluids. J Chem Phys 122:154503

Ballenegger V, Arnold A, Cerda J (2009) Simulations of non-neutral slab systems with long-range electrostatic interactions in two-dimensional periodic boundary conditions. J Chem Phys 131:094107

Binder K, Horbach J, Kob W, Paul W, Varnik F (2004) Molecular dynamics simulations. J Phys: Condens Matter 16:S429

Bogusz S, Cheatham TE III, Brooks BR (1998) Removal of pressure and free energy artifacts in charged periodic systems via net charge corrections to the Ewald potential. J Chem Phys 108:7070–7084

Celebi AT, Barisik M, Beskok A (2017) Electric field controlled transport of water in graphene nano-channels. J Chem Phys 147(16):164311

Chan Y, Ren Y (2016) Effects of surface charges on the seawater desalination using functionalized graphene. J Appl Math Phys 4:602

Chen B, Jiang H, Liu X, Hu X (2017a) Molecular insight of water desalination across multilayer graphene oxide membranes. ACS Appl Mater Interfaces 9:22826–22836

Chen B, Jiang H, Liu X, Hu X (2017b) Observation and analysis of water transport through graphene oxide interlamination. J Phys Chem C 121:1321–1328

Cipcigan FS, Sokhan VP, Jones AP, Crain J, Martyna GJ (2015) Hydrogen bonding and molecular orientation at the liquid–vapour interface of water. PCCP 17:8660–8669

Cohen-Tanugi D, Grossman JC (2012) Water desalination across nanoporous graphene. Nano Lett 12:3602–3608

Daub CD, Bratko D, Leung K, Luzar A (2007) Electrowetting at the nanoscale. J Phys Chem C 111:505–509

Ewald PP (1921) Die Berechnung optischer und elektrostatischer Gitterpotentiale. Ann Phys 369:253–287

Falk K, Sedlmeier F, Joly L, Netz RR, Bocquet L (2010) Molecular origin of fast water transport in carbon nanotube membranes: superlubricity versus curvature dependent friction. Nano Lett 10:4067–4073

Fanourgakis GS, Medina J, Prosmiti R (2012) Determining the bulk viscosity of rigid water models. J Phys Chem A 116:2564–2570

Ghorbanian J, Beskok A (2016) Scale effects in nano-channel liquid flows. Microfluid Nanofluid 20:121

Ghorbanian J, Celebi AT, Beskok A (2016) A phenomenological continuum model for force-driven nano-channel liquid flows. J Chem Phys 145:184109

Giovambattista N, Debenedetti PG, Rossky PJ (2007) Effect of surface polarity on water contact angle and interfacial hydration structure. J Phys Chem B 111:9581–9587

González MA, Abascal JL (2010) The shear viscosity of rigid water models. J Chem Phys 132:096101

Ho TA, Striolo A (2013) Polarizability effects in molecular dynamics simulations of the graphene–water interface. J Chem Phys 138:054117

Ho TA, Striolo A (2014) Molecular dynamics simulation of the graphene–water interface: comparing water models. Mol Simul 40:1190–1200

Hockney RW, Eastwood JW (1988) Particle-Particle-Particle-Mesh (P3m) Algorithms. Computer simulation using particles. Taylor & Francis, Bristol, PA, pp 267–304

Hub JS, de Groot BL, Grubmüller H, Groenhof G (2014) Quantifying artifacts in Ewald simulations of inhomogeneous systems with a net charge. J Chem Theory Comput 10:381–390

Israelachvili JN (2015) Intermolecular and surface forces. Academic press, London

Joseph S, Aluru N (2008) Why are carbon nanotubes fast transporters of water? Nano Lett 8:452–458

Kalluri RK, Konatham D, Striolo A (2011) Aqueous NaCl solutions within charged carbon-slit pores: partition coefficients and density distributions from molecular dynamics simulations. J Phys Chem C 115:13786–13795

Karniadakis G, Beskok A, Aluru N (2005) Simple fluids in nanochannels. Springer, Berlin

Koklu A, Li J, Sengor S, Beskok A (2017) Pressure-driven water flow through hydrophilic alumina nanomembranes. Microfluid Nanofluid 21:11

Koplik J, Banavar JR (1995) Continuum deductions from molecular hydrodynamics. Ann Rev Fluid Mech 27:257–292

Koumoutsakos P, Jaffe R, Werder T, Walther J (2003) On the validity of the no-slip condition in nanofluidics. In: Laudon M (ed) 2003 Nanotechnology Conference and Trade Show, vol 1.

Computational Publications. San Francisco, California, USA, pp 148–151
Kumar Kannam S, Todd B, Hansen JS, Daivis PJ (2012) Slip length of water on graphene: limitations of non-equilibrium molecular dynamics simulations. J Chem Phys 136:024705
Lee CY, McCammon JA, Rossky P (1984) The structure of liquid water at an extended hydrophobic surface. J Chem Phys 80:4448–4455
Li Y, Xu J, Li D (2010) Molecular dynamics simulation of nanoscale liquid flows. Microfluid Nanofluid 9:1011–1031
Lyklema J (2005) Fundamentals of interface and colloid science: soft colloids, vol 5. Academic press, London
Mahmoud KA, Mansoor B, Mansour A, Khraisheh M (2015) Functional graphene nanosheets: the next generation membranes for water desalination. Desalination 356:208–225
Miyamoto S, Kollman PA (1992) SETTLE: an analytical version of the SHAKE and RATTLE algorithm for rigid water models. J Comput Chem 13:952–962
Montessori A, Amadei C, Falcucci G, Sega M, Vecitis C, Succi S (2017) Extended friction elucidates the breakdown of fast water transport in graphene oxide membranes. EPL (Europhysics Letters) 116:54002
Nagayama G, Cheng P (2004) Effects of interface wettability on microscale flow by molecular dynamics simulation. Int J Heat Mass Transf 47:501–513
Nicholls WD, Borg MK, Lockerby DA, Reese JM (2012) Water transport through (7, 7) carbon nanotubes of different lengths using molecular dynamics. Microfluid Nanofluid 12:257–264
Plimpton S (1995) Fast parallel algorithms for short-range molecular dynamics. J Comput Phys 117:1–19
Plimpton S, Pollock R, Stevens M (1997) Particle-Mesh Ewald and rRESPA for Parallel Molecular Dynamics Simulations. In: Proceedings of the eighth SIAM conference on parallel processing for scientific computing, p 8e21
Puah LS, Sedev R, Fornasiero D, Ralston J, Blake T (2010) Influence of surface charge on wetting kinetics. Langmuir 26:17218–17224
Qiao R, Aluru N (2003) Ion concentrations and velocity profiles in nanochannel electroosmotic flows. J Chem Phys 118:4692–4701
Qiao R, Aluru N (2004) Charge inversion and flow reversal in a nanochannel electro-osmotic flow. Phys Rev Lett 92:198301
Radha B et al. (2016) Molecular transport through capillaries made with atomic-scale precision arXiv preprint arXiv:160609051
Sofos F, Karakasidis T, Liakopoulos A (2009) Transport properties of liquid argon in krypton nanochannels: anisotropy and non-homogeneity introduced by the solid walls. Int J Heat Mass Transf 52:735–743
Tazi S, Boţan A, Salanne M, Marry V, Turq P, Rotenberg B (2012) Diffusion coefficient and shear viscosity of rigid water models. J Phys: Condens Matter 24:284117
Thomas JA, McGaughey AJ, Kuter-Arnebeck O (2010) Pressure-driven water flow through carbon nanotubes: insights from molecular dynamics simulation. Int J Therm Sci 49:281–289
Travis KP, Todd B, Evans DJ (1997) Departure from Navier–Stokes hydrodynamics in confined liquids. Phys Rev E 55:4288
Vo TQ, Barisik M, Kim B (2015) Near-surface viscosity effects on capillary rise of water in nanotubes. Phys Rev E 92:053009
Wei N, Peng X, Xu Z (2014a) Breakdown of fast water transport in graphene oxides. Phys Rev E 89:012113
Wei N, Peng X, Xu Z (2014b) Understanding water permeation in graphene oxide membranes. ACS Appl Mater Interfaces 6:5877–5883
Werder T, Walther JH, Jaffe R, Halicioglu T, Koumoutsakos P (2003) On the water–carbon interaction for use in molecular dynamics simulations of graphite and carbon nanotubes. J Phys Chem B 107:1345–1352
Xia X, Berkowitz ML (1995) Electric-field induced restructuring of water at a platinum-water interface: a molecular dynamics computer simulation. Phys Rev Lett 74:3193
Xiao K, Zhou Y, Kong XY, Xie G, Li P, Zhang Z, Wen L, Jiang L (2016) Electrostatic-charge- and electric-field-induced smart gating for water transportation. ACS Nano 10:9703–9709
Xiong W, Liu JZ, Ma M, Xu Z, Sheridan J, Zheng Q (2011) Strain engineering water transport in graphene nanochannels. Phys Rev E 84:056329
Xu WL, Fang C, Zhou F, Song Z, Liu Q, Qiao R, Yu M (2017) Self-assembly: a facile way of forming ultrathin, high-performance graphene oxide membranes for water purification. Nano Lett 17:2928–2933
Yacoby A (2011) Graphene: tri and tri again. Nat Phys 7:925